The Parameterization of the Wave Boundary Layer*

D. CHALIKOV

Marine Prediction Branch, National Meteorological Center, Washington, D.C.

(Manuscript received 12 July 1993, in final form 11 October 1994)

ABSTRACT

An overview of the theory and parameterization of the wave boundary layer (WBL), which is central to small-scale ocean–atmosphere dynamical interactions, is presented. Surface boundary conditions and the form for the local tangential law are then suggested. The corresponding structure of the WBL above a wave field is illustrated using the JONSWAP spectrum as an example. An analytical model of the stationary boundary layer is constructed. It is shown that close to the surface the wind speed profile is nonlogarithmic, and the mean shear stress is not a quadratic function of wind speed. The roughness parameter has its sense only outside of the WBL. The partitioning of momentum flux between turbulence and wave-induced motions is strongly dependent on the assumed upper frequency bound for the wave spectrum. Finally, an algorithm for the parameterization of the WBL in coupled atmosphere–ocean and atmosphere–wave models is suggested.

1. Introduction

Until recently, investigations of the marine boundary layer were based on the usual theory of a boundary layer above an infinite, flat, rigid surface. In fact, the presence of waves was considered only a minor inconvenience forcing one to modify the roughness parameter. No one was puzzled that the roughness parameter is about four orders of magnitude smaller than the height of waves, and no one discussed the treatment of the wind profile at low heights in the presence of finite amplitude waves. Generalizations of the experimental data on the roughness parameter and the drag coefficient were made based on different qualitative hypotheses. The most sophisticated scheme was suggested by Kitaigorodskii (1962), who assumed that roughness may be treated as a spectral decomposition of moving wave obstacles whose contribution depends on the relation of their phase velocity to the wind speed. The problem with this scheme is that it represents the concept of roughness too literally. In reality, this quantity characterizes something that does not exist, namely a parameter introduced into the wind profile to obtain the needed wind velocity. Close to the surface this representation is not valid and a roughness parameter is not meaningful. Essentially, the use of a roughness parameter is only possible at heights much larger than the roughness elements themselves. [See also a discussion of this problem in Chalikov (1993).]

The *wave boundary layer* (WBL) is the lower part of the atmospheric boundary layer above the sea, whose structure is influenced directly by surface waves. Within the WBL, some portion of momentum transfer results from wave-produced fluctuations of pressure, velocity, and stresses. We call this constituent the *wave-produced momentum flux* (WPMF). The typical height of the WBL is

$$h_{\mathrm{WBL}} \approx k_p^{-1} = g\omega_p^{-2}, \tag{1.1}$$

where k_p and ω_p are the peak wavenumber and frequency of the wave spectrum and g is the gravitational acceleration. Estimate (1.1) for h_{WBL} was obtained directly from numerical modeling of wave-produced motions based on the two-dimensional Reynolds equations (Chalikov 1986). Using the Pierson–Moskowitz spectrum for estimation of significant wave height H_s, it follows that

$$\frac{h_{\mathrm{WBL}}}{H_s} = 3.7, \tag{1.2}$$

so the WBL height h_{WBL} is several times larger than the characteristic wave height. Moreover, the main dynamic atmosphere–ocean interaction takes place in the lowest part of the WBL within a height of about H_s, and the structure of the WBL cannot be described in Cartesian coordinates. The most important conclusion of our previous investigation is that all 2D and 3D models of the WBL have to be constructed in a curvilinear coordinate system (also denoted "surface following" coordinates in this paper). The 1D parameterized models of the WBL

* Ocean Prediction Center Contribution Number 75.

Corresponding author address: Prof. Dmitry Chalikov, National Meteorological Center, World Weather Building, W/NMC 2, 5200 Auth Road, Washington, DC 20233.

should be derived from 3D Reynolds equation in a surface-following coordinate system.

A rigorous verification of numerical simulations of the lowest part of the WBL above the wave surface is only possible using measurements made in surface-following coordinates ζ. Unfortunately, such measurements are very complicated even in wind–wave tunnels. Therefore, in practical terms, 2D and, of course, 3D modeling remains the main source of information on the fine structure of the WBL just above the water surface. However, this does not mean that WBL theory is completely unsupported by experimental data. We have previously shown that, due to the fast attenuation of correlations between geometrical characteristics of the surface and fluctuations in the air flow, the differences between ζ and z coordinates disappear with increasing distance from the interface (see Fig. 10 in Chalikov and Belevich 1993, hereafter ChB93). Consequently, the usual experimental data on wind profile and wind stress outside the lowest part of the WBL are appropriate for verifying the integral properties of drag formation. In this paper we formally use a z notation for the vertical axis, assuming that the surface-following coordinate ζ quickly approaches the usual height above the mean water level.

The most important dynamical characteristic of air–sea interaction is the drag coefficient C

$$C = \frac{|T|}{|u|^2}, \tag{1.3}$$

where T is the turbulent stress divided by air density and u is the wind velocity at some reference height. In practice, the reference height is often $z = 10$ m.

Let us suppose for simplicity that the wave field in deep water is produced by a uniform stationary wind velocity u and stress T outside the WBL. In this case, Kitaigorodskii's (1962) similarity approach is valid, and the drag coefficient C at height z should be a function of z, wind velocity $u(z)$, gravitational acceleration g, and the nondimensional parameters that characterize wave maturity, for example, the nondimensional time $\tilde{t} = tg/u$. Alternately, the time-independent variation of sea state as a function of fetch under the action of wind blowing perpendicularly to a shoreline may also be considered. In this case, dimensionless fetch $\tilde{x} = xg/u^2$, rather than dimensionless time $\tilde{t}$, characterizes spectral wave maturity. Finally, a parameterized spectrum, such as the JONSWAP form of Hasselmann et al. (1973), requires other parameters such as the nondimensional peak frequency $\tilde{\omega}_p = \omega_p v_*/g$, where $v_* = |T|^{1/2}$ is the friction velocity. From dimensional considerations and (1.3) we obtain that

$$C = \frac{|T(z)|}{|u^2(z)|} = f\left(\frac{gz}{u^2}, s_w\right), \tag{1.4}$$

where s_w represents a dimensionless parameter characterizing spectral wave maturity.

Equation (1.4) implies that for a given s_w, the drag coefficient C should be a universal function of nondimensional height $\tilde{z} = gz/u^2$. Unfortunately, experimental data stratified over wave age are rare. Exceptions are Donelan (1982) and the recent HEXOS data of Smith et al. (1992). These observations have a large associated scatter. Of course, the most important reasons for this scatter are the nonstationarity and nonhomogeneity of the flow and the density stratification, which create deviations in the self-similar structure outside the WBL. Inside the WBL, deviations also arise due to the generation of wave-produced momentum flux (WPMF), which affects the logarithmic profile and, strickly speaking, makes the roughness parameter meaningless. Nevertheless, the HEXOS data exhibits certain regularities: the drag coefficient increases with wind velocity and decreases with wave age. Specifically, the drag coefficient C_{10} may vary in a range $(1.0–3.0) \times 10^{-3}$, and young sea is much "rougher" than old sea. This may be explained by the strong dependence of the wind–wave interaction parameter β on frequency and on the overshoot effect, which therefore provides the much larger level of energy at high frequencies for young waves than for old ones. Moreover, fast waves, which have wave age c/u close to 1.0, do not create drag, whereas the drag due to slowly moving waves is similar to that resulting from stationary obstacles and is thus very effective. Therefore, the main part of the momentum flux is concentrated at high frequencies and strongly depends on the level of energy there.

In the case of arbitrary two-dimensional directional spectra containing wind waves and swell, the drag coefficient depends on the entire spectrum

$$C = \frac{|T|}{|u|^2} = f\left(\frac{gz}{|u|^2}, S(\omega, \theta)\right). \tag{1.5}$$

An alternate and more convenient representation of sea surface roughness is found in the nondimensional roughness parameter $\tilde{z}_0$, which formally is connected to C by the relation

$$\tilde{z}_0 = \frac{z_0 g}{|T|} = \tilde{z} \exp(-kC^{-1/2}), \tag{1.6}$$

where $\tilde{z}$ is any height normalized by Charnock's scale $\mathcal{L} = |T|/g$, and k is the von Kármán constant.

Outside the WBL where the WPMF is absent, the stress T is a constant with respect to height, and the roughness parameter z_0 approaches a constant, which we call *total* roughness parameter z_{0t}. This quantity reflects the complete mechanism of drag formation arising above the surface. For a fully developed sea, (1.5) then gives the Charnock (1955) relation

$$z_{0t} = m\mathcal{L}, \tag{1.7}$$

where a commonly accepted value for m is 0.0144 (Garrat 1977). In general, parameter m depends on

the entire spectrum and, in more simple situations, on the parameter s_w. In fact, use of the Charnock scale $\mathcal{L}$ allows us to exclude the direct influence of the wind velocity and to stratify the nondimensional roughness in terms of wave state characteristics.

The question often arises as to what part of the momentum is transferred to the waves and what part goes directly to currents. [See Janssen (1989) and discussion in Chalikov (1993).] An answer to this question is possible only when the wave spectrum goes to zero at low frequencies, for example, when only swell is present and the wind is weak. In this situation, the surface is smooth below some frequency and some portion of momentum transfers through the viscous sublayer directly to the horizontal flow of the water. In all other cases, the wind and the nonlinear interactions create a continuous wave spectrum that reaches very high frequencies. In the latter situation, consideration of the relation between wave-form stress and tangential stress is useless because this relation depends only on an arbitrary cutoff frequency ω_c that separates the modeled waves themselves and subgrid disturbances, which we proclaim to be the "roughness elements." If the wave energy density is large and the cutoff frequency ω_c is high enough, the WPMF is close to the total momentum flux in the vicinity of the surface, and the mean tangential stress is very small. However, there is still momentum transfer to currents because the waves dissipate, break, and transfer their momentum to currents. Certainly the timescale of this transition depends implicitly on the spectral wave dissipation timescale.

The most difficult problem of one-dimensional modeling of the WBL is in assigning boundary conditions at the water surface. We can accept the condition of a velocity vector discontinuity at the interface when high frequency waves are absent. But even in this case this condition is difficult to model because the grid has to be fine enough to resolve the viscous sublayer. More importantly, we are forced in this case to speculate on the dynamics at heights on the order of the roughness parameter. Thus, it is very convenient to assume local homogeneity and stationarity for the thin near-surface layer and to use the drag law for tangential stress (Gent 1977; Chalikov 1976, 1978, 1986). We note that the existence of a constant flux sublayer in a case of smooth surface may be proven from the two-dimensional equations of the WBL.

A continuous spectrum with a fully developed but poorly known high-frequency region is much more complicated. First, we cannot resolve all the waves because we do not know their spectrum or drag properties. Second, the dynamic properties of these waves may be very complicated. Yuen and Lake (1982) showed that for a frequency 2–3 times larger than the peak frequency ω_p, the linear dispersive relation is not valid. A direct modeling of nonlinear wave dynamics by Chalikov and Liberman (1991), based on the primitive equations for potential motion with a free surface, also proves that the phase speed c of high frequency waves varies in time with a temporal variance that grows quickly with increasing frequency. Probably this effect may be explained by the presence of bound waves running with the same phase velocity as their "parent" wave. In any case, the structure of high-frequency range is too complicated to be taken directly into account in the formulation of lower WBL boundary conditions. Even the position of the surface is known only to an accuracy of the order of the height of unresolved waves. Therefore, a bulk parameterization of tangential stress in the near-surface layer becomes unavoidable. In Gent and Taylor (1976) and in our previous 2D and 1D models, the quadratic drag law was used. We show below that this approach is acceptable when the height where boundary conditions are assigned is not too small.

It is well known that each wave is associated with a WPMF in a layer thickness of order g/ω^2. The near-surface layer in the presence of a well-pronounced spectral "tail" cannot be considered a constant turbulent flux layer because, as the surface approached, the new evolving waves are involved in drag formation. Therefore, as the distance to the surface decreases, the WPMF increases. To satisfy the momentum balance condition, the turbulent stress also must be decreasing. Our previous calculations for the high-frequency region of the spectrum (ChB93), based on results of two-dimensional modeling, showed that the WPMF increases linearly with respect to the logarithm of height. ChB93 could not give an explanation for this result but simply assigned a lower boundary condition in the form of a quadratic drag law. The local roughness parameter was chosen by estimating the characteristic height of subgrid waves assuming a Phillips spectrum. A more careful consideration of the near-surface dynamic structure is shown in this paper to allow the establishment of a nonlogarithmic wind profile and a drag relation that is not quadratic. These results follow from assuming that close to the surface not only does the spectrum have a universal structure, but the form for the WPMF and the wind profiles are also universal and not directly dependent on the low-frequency region of the spectrum. Properties of the equilibrium range lead to the specification of the local drag law, which connects wind velocity, turbulent stress, and the vertical gradient of the WPMF. The local drag law provides the lower boundary conditions for one-dimensional models of the WBL and upper boundary conditions for the currents in a mixed layer.

The modeling of WBL–waves–mixed layer system, as a whole, is especially important in a coastal zone where the mutual exchange of momentum and energy between wind, waves, currents, and turbulence is very extensive. The formulation of this approach has been discussed in (ChB93). In this study we formulate a

simple one-dimensional WBL model intended for ocean–atmosphere coupling. In a forthcoming paper, we consider the coupling of the WBL-model with a third-generation wave prediction model and a simple model of currents in a mixed layer.

2. Basic equations

The 1D structure of the nonstationary wave boundary layer is governed by the equation

$$\frac{\partial u_i}{\partial t} = \frac{\partial}{\partial z}(T_i + \tau_i), \quad i = 1, 2, \tag{2.1}$$

where z is a vertical coordinate; u_i is the vector components of wind velocity; and T_i and τ_i are vector components of vertical fluxes of momentum produced by turbulence and wave-induced perturbations of pressure, velocity, and stress fields (WPMF) as shown by Chalikov (1978). Height z may be considered as a water-surface-following coordinate (ChB93). Fluxes T_i and τ_i may be expressed in the form

$$T_i = K\frac{\partial u_i}{\partial z}, \tag{2.2}$$

where K is the coefficient of turbulent viscosity.

Assume that τ is a superposition of "elementary" fluxes produced by all waves with frequencies ω and angles θ with respect to the wind:

$$\tau_i = g\int_0^{\omega_r}\int_{-\pi}^{\pi} \mathcal{F} d\theta d\omega,$$

$$\mathcal{F} = k_i S(\omega, \theta)\beta(\tilde{\omega}_a, C_\lambda)F(\xi, \tilde{\omega}_a, C_\lambda). \tag{2.3}$$

Here $\mathcal{F}$ describes the spectral density of WPMF as a function of the nondimensional height ξ

$$\xi = z/\lambda_a, \tag{2.4}$$

nondimensional frequency

$$\tilde{\omega}_a = \omega|u_\lambda|\cos(\theta)/g, \tag{2.5}$$

and the drag coefficient C_λ at height $z = \lambda_a$. In (2.3) k_i are the vector components of wavenumber; $S(\omega, \theta)$ is the two-dimensional wind wave spectrum as a function of frequency ω and angle θ between wind and wave directions; ω_r is the frequency up to which the spectrum S is known (the "cutoff" frequency); and C_λ is the drag coefficient at height $z = \lambda_a$, where

$$\lambda_a = 2\pi g/(\omega^2\cos|\theta|) \tag{2.6}$$

is the so-called apparent wavelength.

In (2.3) β is the nondimensional wind–wave interaction parameter as a function of $\tilde{\omega}_a$ and C_λ. The scalar function $\mathcal{F}$ was investigated in numerical experiments with a 2D model. Because the approximation of this function used in ChB93 was not valid for very high values of drag coefficient, we now use the following expression:

$$\mathcal{F} = \left(1 - \frac{\xi}{(0.1 + 60C_\lambda)}\right)\exp(-10\xi), \tag{2.7}$$

which implies that, in practice, $\mathcal{F}$ depends on the frequency and drag coefficient but not on the wind speed. This means that the nondimensional frequency influences the surface momentum flux τ_0 and the vertical scale λ_a but not its vertical distribution in terms of z/λ_a.

The K-coefficient in (2.2) may be computed by the formula

$$K = kz(e/c_1)^{1/2}, \tag{2.8}$$

where $c_1 = 4.6$ and the equations for turbulent kinetic energy (TKE) may be written in the form

$$\frac{\partial e}{\partial t} = K\frac{\partial u_i}{\partial z}\frac{\partial u_i}{\partial u_i} + \tau_i\frac{\partial u_i}{\partial z} + \frac{\partial}{\partial z}K\frac{\partial e}{\partial z} - \frac{(e/c_1)^{3/2}}{kz}. \tag{2.9}$$

Shear production of turbulence is described by the first term on the right side; the mutual transformation of kinetic energy of wave-produced fluctuations and turbulent energy is described by the second. A discussion of the energetic properties of the WBL is given in Panchenko and Chalikov (1984).

Let us estimate the role of the diffusion term by comparing it with the dissipation term:

$$\delta = \left(\frac{\partial}{\partial z}K\frac{\partial e}{\partial z}\right)\frac{kz}{e^{3/2}} \sim k^2\frac{\Delta e}{e}, \tag{2.10}$$

where Δe is the typical deviation of e due to wave-produced perturbations. Calculation shows that $\Delta e/e$ does not exceed 0.2, implying that the typical value of δ is 0.03 and the influence of TKE diffusion is negligibly small.

We now estimate the role of nonstationarity in (2.9). The dissipation timescale for KET, given by $\mathcal{J}_d = kz/e^{1/2}$, may be estimated by substituting $e = c_1 v_*^2$, which leads to

$$\mathcal{J}_d = \frac{k}{c_1^{1/2}}\frac{h}{v_*}, \tag{2.11}$$

where h is a height of layer. The timescale of the WBL relaxation $\mathcal{J}_r$ to change the stress T by the amount ΔT is approximately $uh/\Delta T$. This scale may be represented as

$$\mathcal{J}_r = \frac{h}{\Delta C u}. \tag{2.12}$$

Here ΔC is the variation of drag coefficient due to wave influence and has a typical value of 0.001.

Finally, the timescale for the wave field evolution $\mathcal{J}_w$ is

$$\mathcal{T}_w = (\beta_p \omega_p)^{-1}, \qquad (2.13)$$

where ω_p is a peak frequency and β_p is a typical value of β at ω_p. Assuming that ω_p is of order of 1 and β_p about 10^{-4}, we obtain a quite reasonable value for the timescale of wave field evolution, $\mathcal{T}_w \approx 10^4$ s. Taking into account that the typical value of the WBL height is 10 m and a typical value for the wind speed is 10 m s^{-1}, the resultant relaxation timescale $\mathcal{T}_r$ for the WBL is of order 500–1000 s, an order of magnitude smaller than $\mathcal{T}_w$. It seems that we can neglect the effect of wind nonstationarity and assume that the wind field in the WBL has always been adapted to the wave field. Although this may be correct for calculations of wind wave fields at synoptic scales, it is not correct for smaller scales, especially under conditions of horizontal inhomogeneity as found in mesoscale models. Moreover, this effect also may be large in the coastal zone. The assumption of stationarity does not work when wind and waves are strongly "unadapted" to each other, for example, when the phase velocity is considerably greater than the wind speed or when the prevailing directions of wind and waves are different. In this case, the mutual adaptation of wind and wave fields occur within a timescale of order $\mathcal{T}_r$.

The relation $\mathcal{T}_d/\mathcal{T}_r$ is about 10^{-2}–10^{-3}, implying that the turbulent energy relation (2.9) may be accepted as a stationary balance of dissipation and production terms:

$$\left(K\frac{\partial u_i}{\partial z} + \tau_i\right)\frac{\partial u_i}{\partial z} - \frac{e^{3/2}}{kz} = 0. \qquad (2.14)$$

The model formulated above illustrates our general approach to modeling the WBL–wind–wave (WW) system. The evolution of the wave field may be simulated using a spectral wave model. In this case the evolutionary problem has to be solved step by step, exchanging information between WBL and WW models. The WBL model calculates the spectral density of energy input to waves as in ChB93, while the WW model simulates the evolution of the wave spectrum. As waves develop, the slow evolution of the whole atmospheric boundary layer occurs. In such calculations, it is necessary to assign the boundary conditions at sufficiently large height ($\approx 10^3$ m) and to take into account the Coriolis term. If Eqs. (2.2), (2.3), and (2.14) are used to parameterize the dynamical interaction in an atmosphere–wave system, the evolution of the atmosphere is described with a 3D thermodynamic atmospheric model. In this case, (2.2), (2.3), and (2.14) establish the connection between wind in the lowest level of the atmospheric model and turbulent stress at the same level. These stress components should be taken into account at the next time step in the atmospheric model. The WBL model provides the wave model with the energy flux spectrum density $\mathcal{E}(\omega)$,

$$\mathcal{E}(\omega) = \frac{\rho_a}{\rho_w}\omega S(\omega, \theta)\beta(\tilde{\omega}_a, C_\lambda). \qquad (2.15)$$

The scheme described may be easily generalized by coupling the WBL and WW models with a mixed layer (ML) model. Existing ML models do not take into account waves at all, and therefore they cannot describe the closed balance of momentum and energy. The general approach to modeling the WBL–WW–ML system is described in ChB93.

3. Boundary conditions for the WBL model: Local drag law

Upper boundary conditions are assigned outside the WBL at height $z = h$, where the WPMF attenuates and the vertical structure of boundary layer is close to a self-similar one. At height h, either the wind velocity

$$z = h: \quad u_i = u_{ih} \qquad (3.1)$$

or vertical turbulent momentum flux

$$z = h: \quad T_i = T_{ih} \qquad (3.2)$$

is assigned.

The problem of lower boundary conditions is quite complicated. It cannot be formulated without consideration of some of the properties of solutions at small heights. At the wave surface itself $z = \eta(x_i, t)$, the surface current velocity components are known

$$z = \eta(x_i, t): \quad u_i = u_{i0}(x_i, t). \qquad (3.3)$$

It is difficult to directly use these boundary conditions even in a coordinate-following system because in the vicinity of the surface small-scale perturbations of unknown nature are present. This layer is analogous to part of the boundary layer above a rigid surface adjacent to roughness elements. The difficulty is avoided in a reasonable manner by introducing a local drag law at a small but finite height $z = z_r$:

$$z = z_r: \quad T_i = f(u_i, h_r), \qquad (3.4)$$

where h_r is the appropriate microscale characterizing the surface. For the case of turbulent flow above a rough surface, h_r is the characteristic height of roughness elements associated with roughness parameter z_0

$$z_0 = mh_r, \qquad (3.5)$$

where m is of order 0.01. For rough surfaces, when $z_0 \gg \nu/v_*$ in the constant flux layer, the wind profile is a logarithmic one, and the local drag law takes the form

$$T_i = C(u_j u_j)^{1/2} u_i. \qquad (3.6)$$

In general, the absolute value and direction of the outer stress T_i and total surface stress may be different, which causes the evolution of the wind profile on timescales of order $\mathcal{T}_r$. Furthermore, a developing

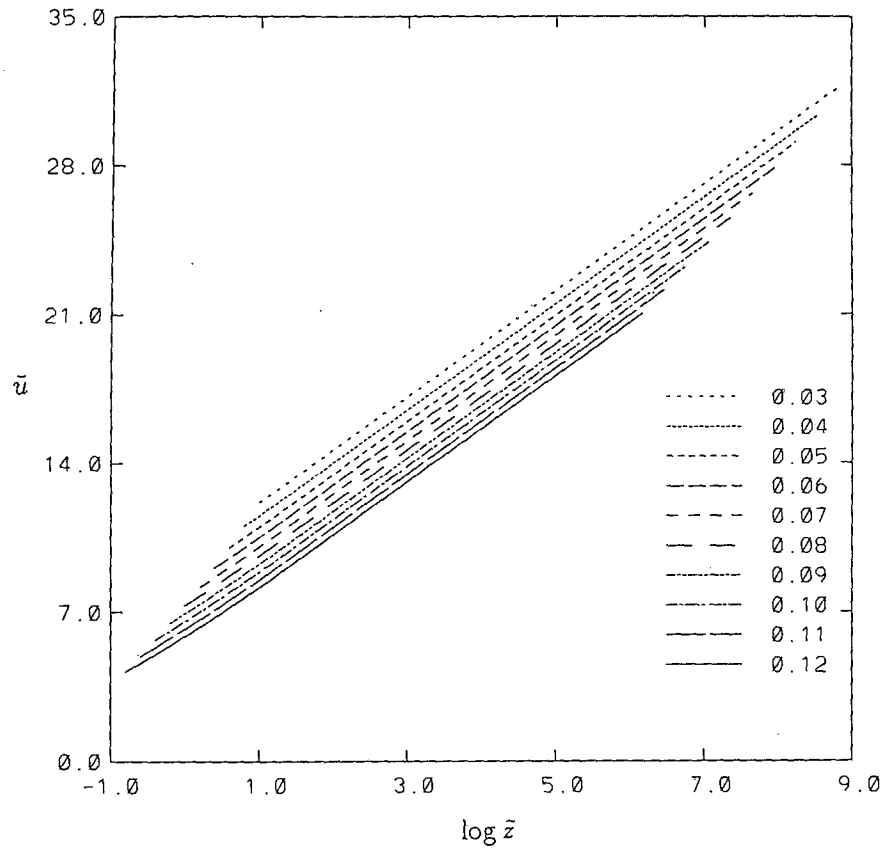

FIG. 1. Wind profiles $\tilde{u}(\tilde{z})$. The curves are labeled by $\tilde{\omega}_p$.

WPMF results in a deviation of the wind profile from a logarithmic variation, implying that a simple quadratic law (3.6) is inappropriate.

Let us consider the lowest part of the WBL adjacent to the water surface at $z < z_a$. The height z_a must be small enough so that the vertical variation of the τ component of the WPMF depends only on waves of the inertial region of the spectrum. In this region, the wave spectral density is assumed to be described by a Phillips law:

$$S(\omega) = \alpha g^2 \omega^{-5}. \tag{3.7}$$

For example, if the wavelength at the spectral peak is about 60 m, the wavenumber is of order 0.1 m^{-1} and the peak frequency is about 1 s^{-1}. If we suppose that the inertial region begins at $3\omega_p$, then z_{in} should be smaller than $g/(3\omega_p)^2 \sim 1$ m. The characteristic height of such waves is also of order 1 m. In this layer we may neglect changes in total stress with height and consider the stationary momentum balance when directions of wind and total stress coincide. We will call this the *adjusted* layer. Aligning the x axis with the wind direction in this layer, we obtain the equation

$$\frac{\partial}{\partial z}(T + \tau) = 0, \tag{3.8}$$

which may be integrated (variables without indexes are assumed to be the absolute values of vectors) to give

$$T + \tau = \text{const} = T_a, \tag{3.9}$$

where T_a is the sum of turbulent and wave-produced stress at height z_a. The equation for turbulent energy may be represented as

$$T_a \frac{\partial u}{\partial z} - \frac{K^3}{(kz)^4} = 0. \tag{3.10}$$

Therefore, the turbulent coefficient may be described by the following expression:

$$K = (kz)^{4/3}\left(T_a \frac{\partial u}{\partial z}\right)^{1/3}. \tag{3.11}$$

Substituting this equation into (3.9) we obtain

$$(kz)^{4/3}(T_a)^{1/3}\left(\frac{\partial u}{\partial z}\right)^{4/3} = T_a - \tau, \tag{3.12}$$

which may be integrated as

$$u = u_r + \frac{T_a^{1/2}}{k}\int_{z_r}^{z}\left(1 - \frac{\tau}{T_a}\right)^{3/4} d\ln z, \tag{3.13}$$

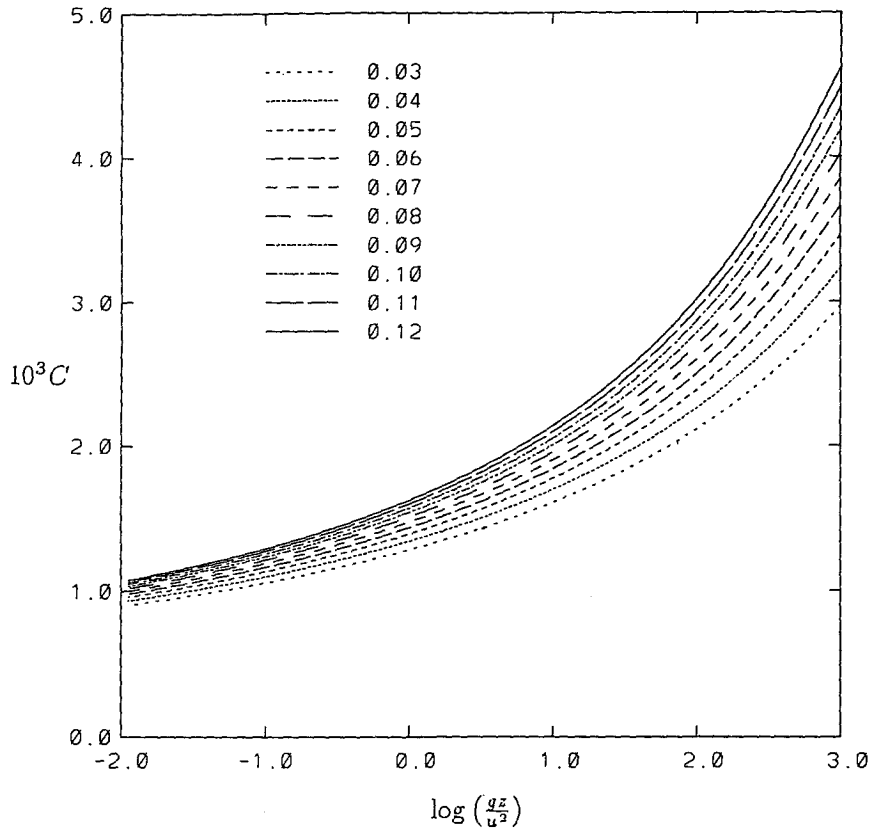

FIG. 2. Drag coefficient profiles $10^3C(u^2/gz)$.

where u_r is a wind velocity at some height $z_r < z_a$. Notice that the wind velocity at any height cannot depend on the choice of an arbitrary reference level z_r, implying that $\partial u/\partial z_r = 0$. The form of u_r in (3.13) is

$$u_r = -\frac{T_a^{1/2}}{k}\int\left(1-\frac{\tau}{T_a}\right)^{3/4} d\ln z + C, \quad (3.14)$$

where C is an integration constant.

Derivation of a wind profile requires establishment of the form of wave-produced stress τ at small heights $z < z_a$. It is natural to suppose that close to the surface the wave-produced momentum stress formed by the universal part of the spectrum (3.7) should be universal too. The absolute value of τ depends on the entire spectrum and cannot be universal. But it is possible to suppose that the vertical derivative of τ close to the surface depends on total local stress, gravitational acceleration g, height z, and parameter α in (3.7), defining the energy density at high frequencies:

$$\frac{\partial\tau}{\partial z} = \varphi(T_a, g, z, \alpha). \quad (3.15)$$

The highest frequency ω_r participating in the formation of τ is related to z by the relation $\omega_r^2 = (g/z_r)$, which is why ω_r is not included in the list of governing parameters. Dimensional considerations imply

$$\frac{\partial\tilde{\tau}}{\partial\tilde{z}} = \psi(\tilde{z}, \alpha), \quad (3.16)$$

where $\tilde{\tau} = \tau/T_a$ and $\tilde{z} = gz/T_a$ are the nondimensional WPMF and height.

Because α is a factor in the spectrum (3.7), it follows from (2.3) that $\partial\tilde{\tau}/\partial\tilde{z}$ depends on α linearly. Taking into account that $T_a/gz \ll 1$, we represent the function ψ by expansion

$$\psi = \alpha\left(a_0 + \frac{a_1}{\tilde{z}} + \frac{a_2}{2\tilde{z}^2} + \cdots\right). \quad (3.17)$$

It is evident that as T decreases to zero, $\partial\tilde{\tau}/\partial\tilde{z}$ must also vanish. Thus, $a_0 = 0$, and the simplest form of (3.17) is

$$\frac{\partial\tilde{\tau}}{\partial\tilde{z}} = \frac{\alpha a_1}{\tilde{z}}. \quad (3.18)$$

Integrating (3.18) we obtain

$$\tilde{\tau} = 1 + \alpha a_1 \ln(z/z_{00}), \quad (3.19)$$

where a_1 is a universal (negative) constant and z_{00} is the height at which τ converges into T_a. Ob-

viously, the sense of z_{00} is similar to that of the roughness parameter z_0 for the wind profile. Formally, z_0 is some (very small) height at which the wind, being log-linearly extrapolated downward, theoretically decreases to zero. In reality, both the interpretation of z_0 in terms of the wind profile and the interpretation of z_{00} in terms of the WPMF are incorrect because we have neglected all effects of molecular viscosity and capillarity. Nevertheless, (3.19) may be useful for analytical representations of the wind profile.

Equation (3.19) has a deep physical sense. It implies that near the surface, contributions to WPMF are due to the smaller and smaller waves. It is remarkable that the considerations presented above were confirmed by numerical calculations of the WPMF profile performed with the JONSWAP spectrum in ChB93. Each WPMF profile revealed a linear dependence of τ on log-z over a broad range of log-heights close to the surface.

Substituting (3.19) in (3.13), we obtain the local drag law for the adjusted layer of the WBL:

$$u_r = \frac{4T_a}{7k}(\alpha a_1)^{3/4}\left(\ln\frac{z}{z_{00}}\right)^{7/4} + C. \quad (3.20)$$

This formula may be represented also in the form

$$u_r = \frac{4T_a}{7k}\left(\frac{\partial\tau}{\partial \ln z}\right)_r^{-1}\left(1-\frac{\tau}{T_a}\right)^{7/4} + C. \quad (3.21)$$

Let us determine the integration constant C. First, note that an expression of type (3.21) describing the wind profile cannot be used directly because, as $\partial\tau/\partial \ln z \to 0$, the wind velocity $u \to \infty$. This contradiction implies that τ and the vertical derivative of τ both converge to zero simultaneously. When the fetch is sufficiently long, the negative fluxes of momentum at low frequencies begin to weaken the positive fluxes of momentum on the medium frequencies and all the WPMF is concentrated at high frequencies. In this case the height of the WBL increases, but WPMF approaches zero, and the sea surface influences the air flow only through its usual roughness. Therefore, we need to introduce the roughness parameter z_0 for wind velocity. Of course, form drag is generated and develops in this situation too, although very close to the surface it is due to surface perturbations of poorly known nature. This type of drag formation approximates that above a solid rough surface. It was found in ChB93 that the nondimensional roughness parameter $\tilde{z}_0$ may be represented in a form

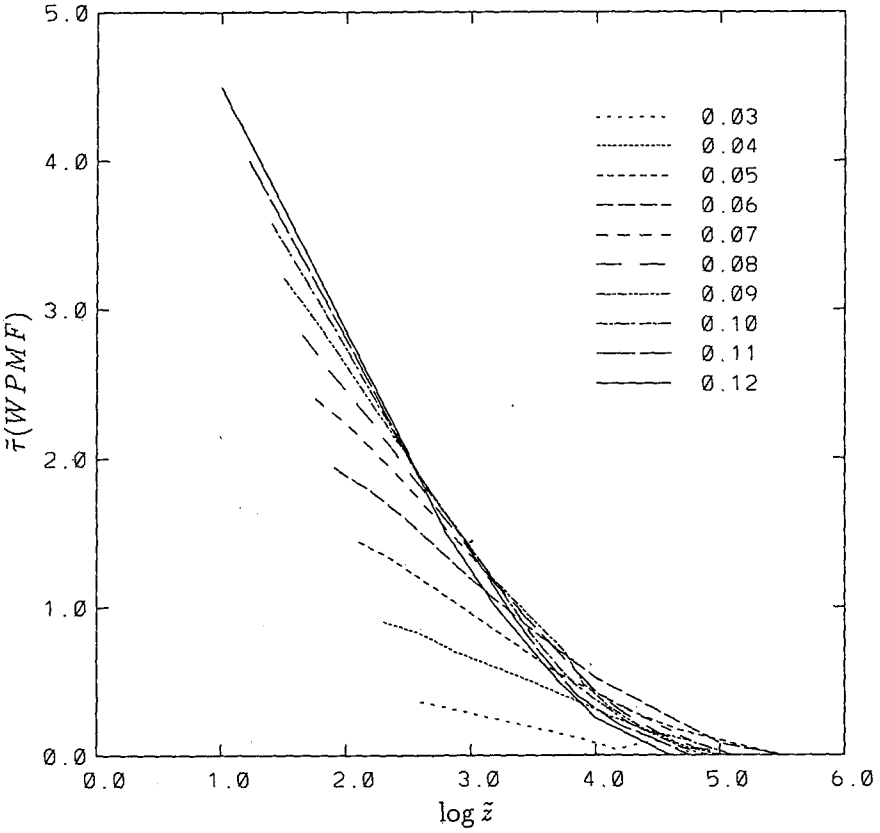

FIG. 3. Wave-produced momentum flux WPMF profiles $\tilde{\tau}(\tilde{z})$.

$$\tilde{z}_0 = z_0 \mathcal{L}^{-1} = \chi\sqrt{\alpha}, \qquad (3.22)$$

where α is a constant in Phillips law (3.7) and χ is a constant. The sense of formula (3.22) is that α characterizes the level of energy in the high-frequency part of the spectrum. As the mechanism of drag formation from high-frequency surface perturbations is unknown, this constant has to be derived from empirical data. An approximate estimate of χ is possible using the Pierson–Moskowitz spectrum with $\alpha = 8.1 \times 10^{-3}$. For $\tilde{z}_0 = m = 0.0130$ (Smith and Banke 1975), 0.0144 (Garret 1977), and 0.0185 (Wu 1980), we have obtained $\chi = 0.14$, 0.16, and 0.20, respectively. ChB93 showed that the wave-induced momentum flux for a fully developed sea is small. Therefore, the wind profile is close to logarithmic even at very small heights. Thus, consider that the total and local roughness parameters are equal to each other.

It is important to emphasize that we are forced to introduce the roughness parameter z_0 only because we do not know the mechanism of drag formation at very high frequencies. Form drag plays the main role for the sufficiently mature or fully developed sea. The specific property of the WBL is that for values $z_{00} > z_0$ the WPMF provides enough stress for the vanishing of the wind at height $z = z_{00}$. In this case the usual roughness parameter does not apply. In its place it is appropriate to use a rule,

$$z_0 = \max(z_0, z_{00}). \qquad (3.23)$$

We are now faced with the problem of how to compute the boundary conditions formulated above in a numerical solution of the WBL one-dimensional problem. Because (2.1)–(2.3) are strongly nonlinear, it is reasonable to solve them iteratively. Let us suppose that τ_r and τ_0 are the values of the WPMF at levels $z = z_r$ and $z = z_0$ and $(\partial\tau/\partial z)_r$, its vertical derivative at $z = z_r$. Then, assigning $u = 0$ at $z = z_0$, we can evaluate the integration constant in (3.14) and represent u_r in the form

$$u_r = -\frac{4}{7k} T_a^{3/2} \left(\frac{\partial\tau}{\partial \ln z}\right)_r^{-1} \times \left[\left(1 - \frac{\tau_r}{T_a}\right)^{7/4} - \left(1 - \frac{\tau_0}{T_a}\right)^{7/4}\right], \qquad (3.24)$$

where τ_0 may be derived from the log-linear distribution of τ in (3.19)

$$\tau_0 = T_a\left(1 + \frac{\partial\tau}{\partial \ln z} \ln\frac{z_0}{z_{00}}\right). \qquad (3.25)$$

It follows immediately that $\tau_0 < T_a$ when $z_{00} < z_0$, which arises above a fully developed sea when wave age c_p/u is close to (or smaller than) unity and the negative flux of energy dominates the low-frequency part of spectrum. In the presence of fast long waves aligned in the direction of the wind, the positive flux from these waves to the wind may considerably decrease the negative momentum flux from the wind to short waves, and the total friction may be weakened. To satisfy the momentum balance condition the wind speed will increase. When a positive WPMF exists, the total roughness parameter becomes less than the local roughness parameter. Of course, the total momentum flux cannot drop to zero, although for very long fetches in the hypothetical situation of an "overdeveloped" sea (as reported empirically by Glazman and Pilorz 1990), the sea surface may become very smooth in the sense of a total roughness parameter. In (3.26), $\tilde{\tau}_r$ and $\tilde{\tau}_0$ are values of WPMF at levels $\tilde{z} = \tilde{z}_r$ and $\tilde{z} = \tilde{z}_0$. For developing sea (according to our calculation when $\omega_p > 0.075$ or $u/c_p > 1.8$) the WPMF can be large enough to equal the outer value of stress T_h, implying that $\tau_0 = 1$. It is remarkable that in this case Eqs. (2.1), (2.15), and the boundary condition (3.26) form a closed system, and information on the local roughness parameter is not needed.

In presenting the boundary conditions for the WBL we proceeded from the assumption that the wind is strong enough to form an inertial subrange in the wave spectrum. However, it is known that the inertial interval cannot arise when the wind is weak. This implies that in the vicinity of the interface the high-frequency WPMF is absent and the turbulent stress is a constant with respect to height. In this regime the drag relation (3.26) is not valid. Therefore, the drag coefficient (1.4) may depend on additional nondimensional parameters that include the molecular viscosity and coefficient of surface tension. Empirical evidence of the growth of

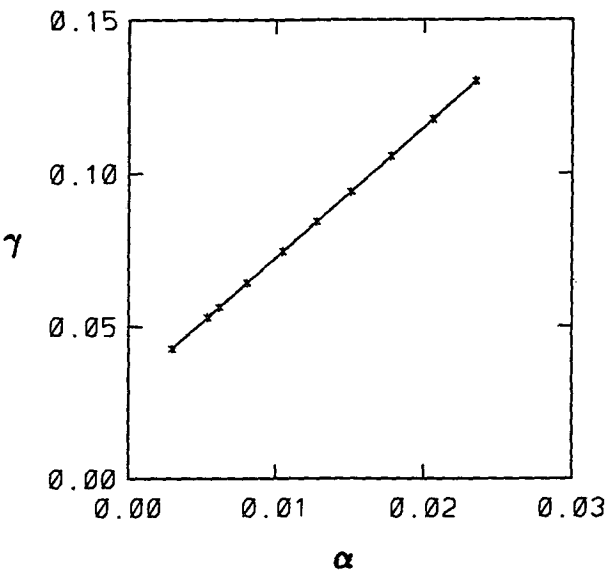

FIG. 4. The dependence of nondimensional gradient of WPMF γ in the adjusted layer on Phillips constant α. Asterisk: calculations and curve: approximation (4.6).

the roughness parameter with decreasing wind are given by Wu (1988) (see also the discussion in Blake 1991). Although this regime may be investigated numerically using a 2D model of the WBL, it has thus far not been completed.

4. Structure of WBL above developing waves

Let us consider the structure of the WBL for the case when the wave field is produced by the local wind in the absence of swell. We suppose that the spectral density distribution as a function of nondimensional frequency $\omega v_*/g$ is described by the JONSWAP approximation (Hasselmann et al. 1973, 1980). The nondimensional peak frequency $\tilde{\omega}_p$ is a parameter of the approximation. Let the axis x be alongwind. Because the JONSWAP spectrum is symmetric relative to the wind, the directions of the turbulent stress and the WPMF coincide with the wind direction. It is convenient to represent the governing equations (2.1)–(2.3) and (2.15) in nondimensional form by the scaling: velocity $v_* = T_h^{1/2}$, length v_*^2/g, turbulent energy v_*^2, turbulent viscosity coefficient v_*^3/g, and wavenumber g/v_*^2. Using the estimate of timescale from (2.12)–(2.14), we consider the stationary one-dimensional WBL problem. In this case, the total stress $T + \tau$ is a constant over height:

$$\tilde{K}\frac{\partial \tilde{u}}{\partial \tilde{z}} + \tilde{\tau} = 1, \tag{4.1}$$

and the momentum balance equation takes the form

$$(k\tilde{z})^{4/3}\left(\frac{\partial \tilde{u}}{\partial \tilde{z}}\right)^{4/3} + \tilde{\tau} = 1, \tag{4.2}$$

where $\tilde{\tau}$ is the nondimensional WPMF

$$\tilde{\tau} = \int_0^{\tilde{\omega}_r}\int_{-\pi}^{\pi} \cos(\theta)\tilde{\omega}^2 S(\tilde{\omega})D(\tilde{\omega}, \theta) \times \beta(\tilde{\omega}_a, C_\lambda)F(\xi, C_\lambda)d\theta d\tilde{\omega}. \tag{4.3}$$

Taking into account the boundary condition (3.24), the integral of (4.2) may be represented in the form:

$$\tilde{u} = -\frac{4}{7k}\left(\frac{\partial \tau}{\partial \ln z}\right)_r^{-1}[(1-\tilde{\tau}_r)^{7/4} - (1-\tilde{\tau}_0)^{7/4}] + \frac{1}{k}\int_{\tilde{z}_r}^{\tilde{z}} (1-\tilde{\tau})^{3/4} d\ln z. \tag{4.4}$$

Although this is not an explicit solution because $\tilde{\tau}$ depends on $\tilde{u}$, this form is convenient for iterations.

Some computations from Eq. (4.1) were presented in ChB93. Those computations did not take into account the universal structure of the WPMF profile formed by the high-frequency part of the spectrum, as expressed by (3.19), but used the local quadratic drag law instead of (3.24). The new results obtained from (4.4) and the boundary conditions (3.2) and (3.24) are shown in Figs. 1–10 for $0.03 \leqslant \tilde{\omega} \leqslant 0.12$. The boundary conditions (3.2) and (3.24) were assigned at $h = 1/\tilde{\omega}_p^2$ and $h_r = 1/\tilde{\omega}_r^2$. The JONSWAP spectrum was approximated using a frequency step $\Delta\tilde{\omega} = \tilde{\omega}_p/20$ up to the "cutoff" frequency $5\tilde{\omega}_p$. Increasing the "cutoff" frequency up to $7\tilde{\omega}_p$ did not change the results significantly. Wind profiles presented in Fig. 1 are almost logarithmic only for an old sea (small $\tilde{\omega}_p$). Beginning from $\tilde{\omega}_p = 0.05$, the wind profile exhibits a deviation from logarithmic variation because of the WPMF (Fig. 3). Thus, a widely used variable such as the drag coefficient C_{10} at $z = 10$ is inconvenient because difficulties in comparison of data referred to other heights. A much more universal variable is the drag coefficient C with its dependence upon nondimensional height gz/u^2 and some characteristic of wave field, such as the nondimensional peak frequency $\tilde{\omega} = v_*/c_p$. This dependence is presented in Fig. 2. It is seen that even for the idealized conditions of stationarity, homogeneity, and the absence of swell the variability of the drag coefficient may be very large. The vertical profiles of the WPMF are shown in Fig. 3. The smaller the peak frequency, the smaller the WPMF at the same height, but the greater the height it reaches because it is produced by longer waves. Closer to the surface, the WPMF grows linearly in log-height in a good agreement with the dependence (3.19) obtained with similarity considerations. Equation (3.19) may also be written as

$$\tilde{\tau} = \gamma \ln\frac{\tilde{z}}{\tilde{z}_1}, \tag{4.5}$$

where $\gamma = \partial\tilde{\tau}/\partial \ln z$ is the gradient of the WPMF in the log-scale and z_1 is the height at which $\tilde{\tau}$ is zero when extrapolated log-linearly. The value of γ depends on the wave spectrum at high frequencies. If the shape of the spectrum at high frequencies is universal, then the definition of the WPMF (2.3) implies that the dependence of γ on the Phillips constant α is almost linear. This dependence is presented in Fig. 4.

The calculations presented in Fig. 4 allow construction of an approximation for the term $\partial\tilde{\tau}/\partial \ln\tilde{z}$ appearing dimensionally in (3.19):

$$-\frac{\partial\tilde{\tau}}{\partial \ln\tilde{z}} = 0.03 + 4.25\alpha. \tag{4.6}$$

This dependence is correct in the range $0 < \alpha < 0.07$. The Phillips constant α may be approximated by the formula (Janssen 1989)

$$\alpha = 0.57\tilde{\omega}_p^{3/2}, \tag{4.7}$$

which applies in the range $0.03 < \tilde{\omega} < 0.25$.

We note that formula (4.6) is needed when we cannot reach high enough resolution for the spectrum and we are not able to calculate $\partial\tau/\partial z$ directly using (2.3).

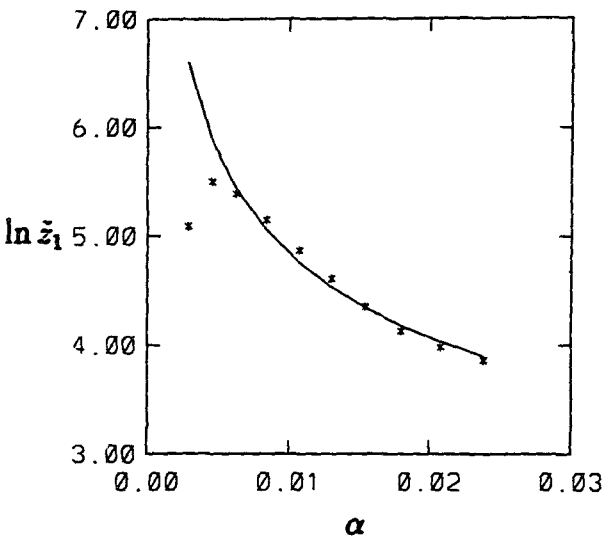

FIG. 5. The dependence of parameter $\tilde{z}_1$ [see (4.8) on Phillips constant α].

In general, formula (3.14) provides the boundary condition for the evolutionary equation (2.1). The dependence of $\ln z_1$ on the peak frequency ω_p is shown in Fig. 5. Although the height z_1, where the WPMF approaches zero, may depend on the long wave part of spectrum, that dependence cannot be universal. Nevertheless, if we suppose that the wind wave spectrum may be described by the JONSWAP spectrum and swell is not important because of its small steepness, estimates from Fig. 5 may be used to approximate the vertical distribution of the WPMF as follows,

$$\ln\tilde{z}_1 = 1.53\alpha^{-1/4}. \tag{4.8}$$

Note that the accuracy of relations typical of (4.6) depends completely on the accuracy of function $\beta(\tilde{\omega}_a, C)$ for large values of C_λ, simply speaking, for small heights. At present time we do not know well enough the shape of β for $C_\lambda > 3 \times 10^{-3}$.

A specific feature of the JONSWAP spectrum (Fig. 6) is the strong "overshoot" effect: energy in the high-frequency part of the spectrum decreases with increasing wave age. To estimate the contribution of different parts of the spectrum in the momentum and energy exchange, we calculate the integrals:

$$I_1(\tilde{\omega}) = \int_0^{\tilde{\omega}}\int_{-\pi}^{\pi} \tilde{\mathcal{E}}_0 d\theta d\omega, \quad I_2(\tilde{\omega}) = \int_0^{\tilde{\omega}}\int_{-\pi}^{\pi} \tilde{\mathcal{F}}_0 d\theta d\omega, \tag{4.9, 4.10}$$

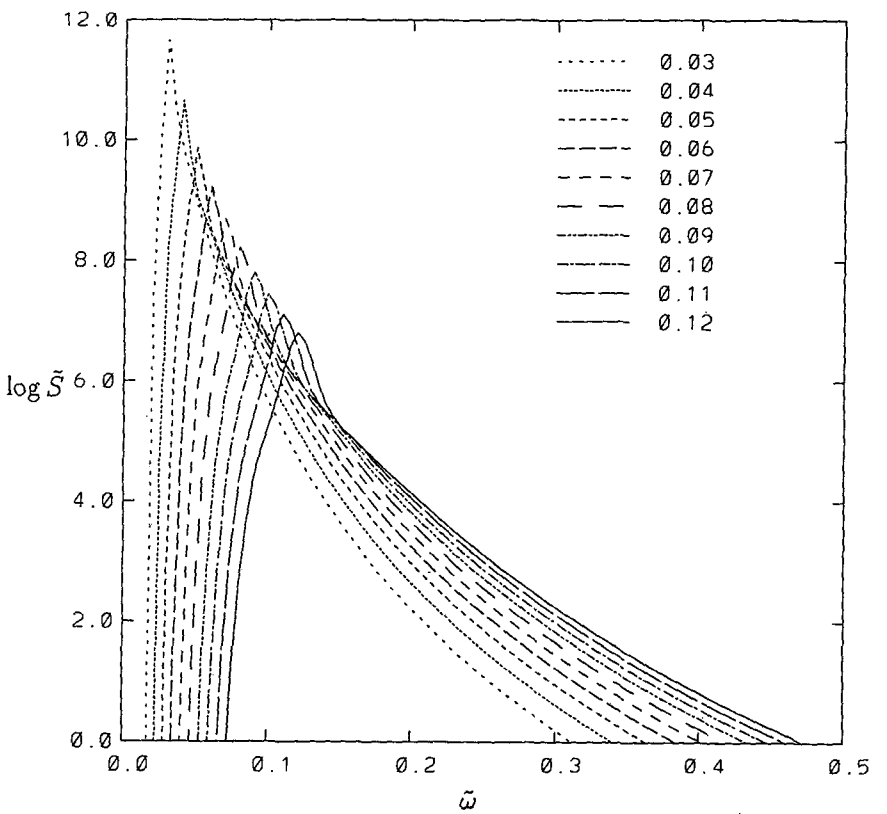

FIG. 6. JONSWAP spectrum.

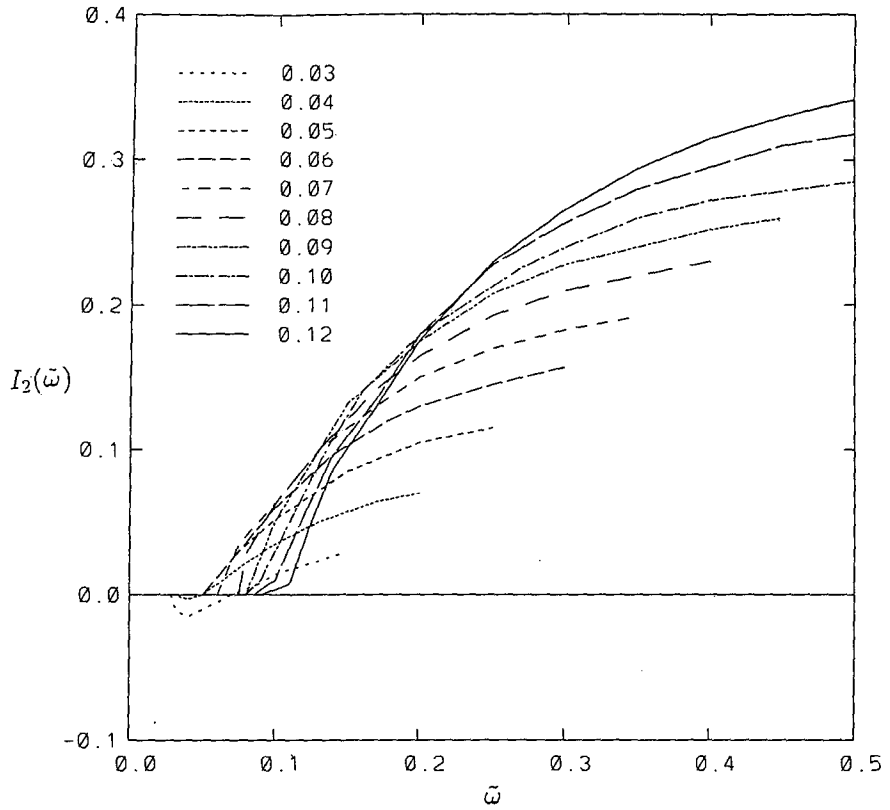

FIG. 7. Momentum flux integral spectrum density $\tilde{\mathcal{E}}(\tilde{\omega})$ [Eq. (4.10)].

where $\tilde{\mathcal{E}}_0$ is the spectral density of energy exchange

$$\tilde{\mathcal{E}}_0 = \tilde{\omega} S(\tilde{\omega}, \theta) \beta(\tilde{\omega}_a, C_\lambda), \qquad (4.11)$$

and $\mathcal{T}_0$ is the spectral density of the momentum exchange at the lowest level of the numerical model $\tilde{z} = \tilde{h}_r$ [see (2.3)]. The dependencies of I_2 and I_1 on frequency $\tilde{\omega}$ are presented in Figs. 7 and 8. It is interesting that the momentum and energy fluxes to waves decrease as the waves develop. An explanation for this phenomena is that the phase velocity approaches the wind velocity, and the wind–wave interaction parameter β goes to zero.

Due to the logarithmic growth of the WPMF approaching the surface, the magnitude of this quantity depends on height. Therefore, consideration of the "surface" value, considered by Janssen (1989) and Jenkins (1992) is not meaningful. Trying to assume that the nondimensional WPMF at the surface is equal to unity is also not constructive. Clearly the integrated momentum flux spectrum density $\tilde{\mathcal{T}}$ is a function of ω_r. The decision concerning what portions of the momentum have to be attributed to waves or currents therefore depends, in practice, on spectral and spatial resolution of the wave models. This implies that waves that disappear at scales on the order of the horizontal grid step give their momentum and energy immediately to the local currents and mixed layer turbulence. In principle, the same effect also takes place for the energy flux, and assuming $S(\omega) \propto \omega^{-5}$ and $\beta \propto \omega^2$ (at high frequencies), the integration of (4.9) over all frequencies formally gives a finite value. Although both momentum and energy fluxes are finite, their values may of course depend on the physics of the high-frequency interaction. Fortunately, we know the limiting value for the momentum flux: for quasi-stationary flow it cannot exceed the external value of T. The analogous balance estimate for the energy flux is not possible because of a singularity in the dissipation in boundary layer.

For long fetches (and mature spectra: $\tilde{\omega} \approx 0.03$), both momentum and energy input are negative at low frequencies because the waves run faster than the wind and they transfer their momentum back to the atmosphere. Although the momentum flux integrated over frequency is, of course, positive, the total energy flux is directed from wind to waves. The dependence of integrated energy flux on the peak frequency is shown in Fig. 9. A sign change occurs at $\tilde{\omega} = 0.035$ and a saturation level $I_1 = 2.1$ is reached at frequency $\tilde{\omega} \approx 0.1$. For very short fetches the limiting value of I_1 then decreases once more, but as this regime is beyond the range of known β-param-

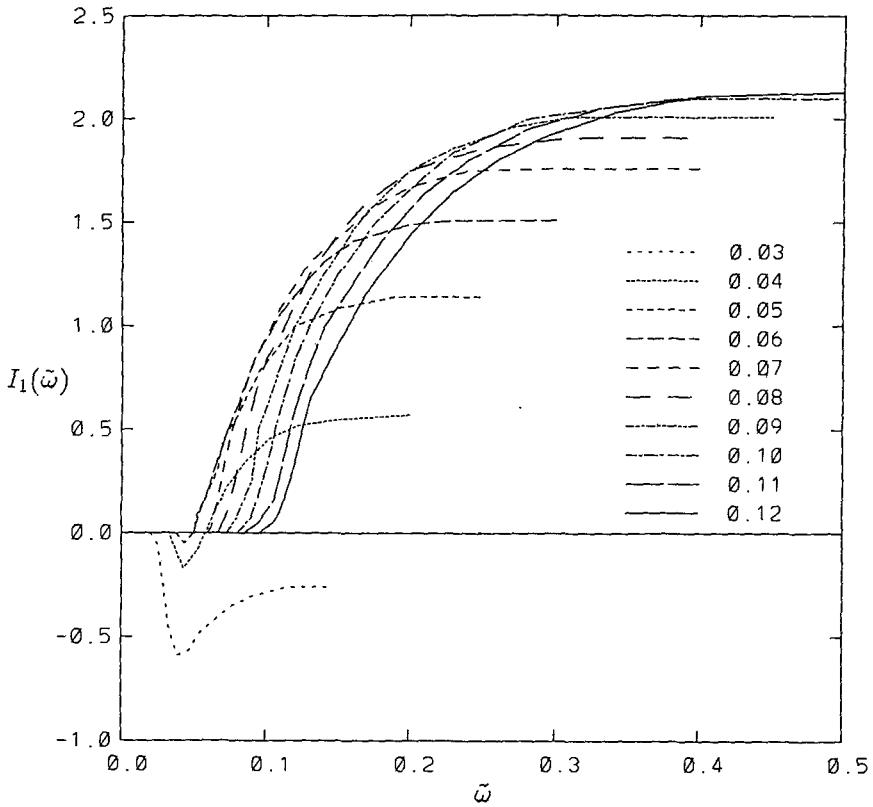

FIG. 8. Energy flux integral spectrum density $I_1(\tilde{\omega})$ [Eq. (4.9)].

eter values, it merits a (future) dedicated investigation. Finally, it may turn out that the negative energy flux arising at low frequencies is the sole reason for a possible stabilization of the wind wave spectrum at fixed wind.

For numerical solution of (2.1)–(2.3), we used a semi-implicit scheme based on (4.4) rewritten in the logarithmic vertical coordinate $\xi = \ln((z-\eta)/z_r)$. The wind and WPMF profiles were calculated iteratively.

Modifications of scheme

The method suggested is very simple and may easily be implemented in coupled ocean–atmosphere models. Nevertheless, this approach may turn out to be too expensive because it is necessary to calculate the integrals over the wave spectrum many times and to solve (2.1)–(2.3) iteratively. A simplified method may be based on the following assumptions.

(i) The WPMF created by swell is small compared with the WPMF produced by wind waves.

(ii) The spectrum of wind-generated waves is similar to the JONSWAP spectrum.

(iii) The structure of the WBL may be described assuming the stationary momentum balance equation.

With these assumptions, we may avoid numerically solving the momentum balance equation (2.1) and use a simple analytical representation of the wind profile under stationary conditions that may be obtained using a symmetric wave spectrum and approximating the WPMF by

$$\tilde{\tau} = \max\left(0, -\gamma \ln \frac{\tilde{z}}{z_1}\right). \tag{4.12}$$

In nondimensional form the solution may be written as

$$\tilde{u} = \begin{cases} -\dfrac{4}{7k\gamma}\left[\left(1-\gamma\ln\dfrac{\tilde{z}}{\tilde{z}_1}\right)^{7/4} - \left(1-\gamma\ln\dfrac{\tilde{z}_0}{\tilde{z}_1}\right)^{7/4}\right] & \text{at } \tilde{z} < \tilde{z}_1 \\ -\dfrac{4}{7k\gamma}\left[1-\left(1-\gamma\ln\dfrac{\tilde{z}_0}{\tilde{z}_1}\right)^{7/4}\right] + \dfrac{1}{k}\ln\dfrac{\tilde{z}}{\tilde{z}_1} & \text{at } \tilde{z} \geq \tilde{z}_1, \end{cases} \tag{4.13}$$

where $\tilde{z}_0$ is defined by (3.24) and

$$\tilde{z}_{00} = z_1 \exp(-\gamma^{-1}). \tag{4.14}$$

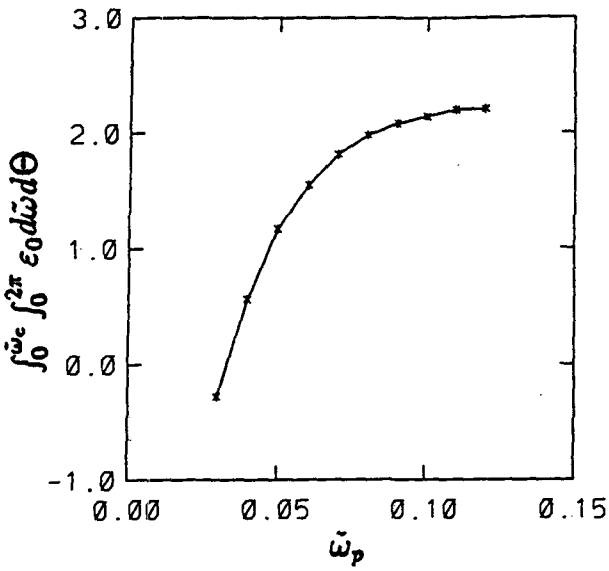

FIG. 9. The nondimensional energy input to waves as function of peak frequency $\tilde{\omega}$.

The analytical solution (4.13) is in a good agreement with the numerical solution (4.3), (4.3). As the WPMF diminishes and $\gamma \to 0$, Eq. (4.13) gives the usual logarithmic profile $\tilde{u} = k^{-1} \ln(\tilde{z}/\tilde{z}_0)$. Outside the WBL the wind profile may be represented as $\tilde{u} = k^{-1} \ln(\tilde{z}/\tilde{z}_{0t})$, where $\tilde{z}_{0t}$ is a total roughness parameter. Equating this formula to (4.13) we obtain

$$\tilde{z}_{0t} = \tilde{z}_r \exp\left\{-u_r + \frac{1}{k}\int_{\tilde{z}_r}^{\tilde{z}} [1 - (1 - \tilde{\tau})^{3/4}] d \ln z\right\}. \tag{4.15}$$

The first term in braces gives the contribution of the high frequency "tail," while the second gives the contribution of the discrete region of the spectrum. Although the values of these terms depend on the assumed height $\tilde{z}_r$ of the parameterized near-surface layer, the value of the total roughness parameter z_{0t} does not depend on $\tilde{z}_r$ at all because of the definition of the local drag law (3.14) and the universality of the WPMF profile (3.19). It is evident that at $\tilde{\tau} = 0$ the total roughness parameter is equal to the local roughness parameter that is created by the high frequency tail. When the $\tilde{\tau}$ component of the WPMF is positive, the total roughness parameter increases due to additional drag produced by the waves. At $\tilde{\tau} < 0$ the WPMF directed from waves to wind makes the total roughness parameter smaller than the local roughness parameter.

In general, when the wave spectrum contains waves and swell running at different angles to the wind, the vector of total momentum flux on the surface does not coincide with the momentum flux outside the WBL. In this case the interaction is much more complicated and cannot be described, assuming a stationary approach. Nevertheless, for a very thin adjusted layer above the surface the assumption of stationarity is valid, and the local drag law (3.21) may be used as a lower boundary condition for the nonstationary problem. In this case we assumed that if wind is not weak, the high-frequency part of spectrum governing the local roughness is formed by the local wind.

The solution (4.13) may be used for calculating a stationary wind profile up to small heights in a sea-surface-following coordinate system. This wind profile may be used for calculations of energy input up to very high frequencies. In fact, the existing wave models are the "large wave models": they are unable to take into account very short waves because of computational restrictions. For example, the length of the shortest wave in a global version of the WAM model is about 15 m, so the height where wind–wave interaction takes place is much higher than the depth of the layer where the log-profile of τ exists. In this case the fine details of the wind profile are insignificant, and it may be approximated by

$$u(z) = \frac{v_*}{k} \ln \frac{z}{z_{0t}}. \tag{4.16}$$

Principally, z_{0t} may be derived from (4.15), but it is more convenient to use the next simple procedure, which is based on relation (3.22).

The drag coefficient and consequently energy input to all waves in the scheme described depends on the shape of the high frequency tail. For the JONSWAP spectrum the Phillips parameter α is connected with the peak frequency by relation (4.7); it may be assumed that some rule exists for the evaluation of c_p in the computed 2D spectrum. For example, we may suppose that ω_p is the highest and closest to the wind direction maximum in the spectrum $S(\omega, \theta)$. Another way to determine α may be based on direct calculation of α by approximation of the modeled spectrum tail by ω^{-5} law. (Note that for an arbitrary wave field, a much more informative characteristic than wave peak frequency may be the frequency of peak input energy).

Formula (4.16) may be rewritten in terms of a drag coefficient C:

$$C = k^2[R - \ln(C)]^2, \tag{4.17}$$

where

$$R = \ln\left(\frac{zg}{\chi\sqrt{\alpha u^2}}\right) \tag{4.18}$$

is a nondimensional parameter and z is an arbitrary height.

Equation (4.18) was solved analytically, and its solution shown in Fig. 10 was approximated with formula

$$C = 10^{-3}\left(0.021 + \frac{10.4}{R^{1.23} + 1.85}\right) \tag{4.19}$$

in the range $-1.0 < R < -8.0$.

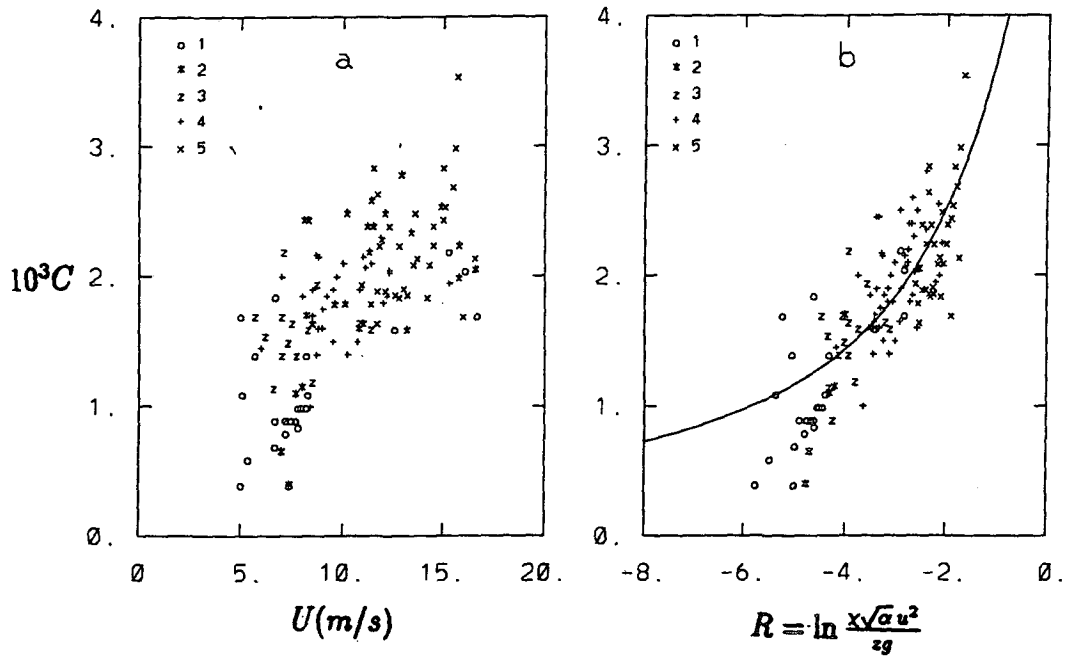

FIG. 10. The empirical dependence of drag coefficient C on wind velocity U_{10} (Donelan 1982) (a) and on nondimensional parameter R (b). 1) $0.8 < \tilde{\omega}_a < 1.5$; 2) $1.5 < \tilde{\omega}_a < 2.0$; 3) $2.0 < \tilde{\omega}_a < 3.0$; 4) $3.0 < \tilde{\omega}_a < 4.0$ and 5) $4.0 < \tilde{\omega}_a < 6.0$.

Thus, the dependence of the drag coefficients $C(z)$ on wind velocity $u(z)$ and sea state, expressed in terms of the Phillips coefficient α, may be reduced to the dependence on a single parameter R. Unfortunately, the empirical data on the dependence of the drag coefficient or roughness parameter on fetch are scarce. To verify formula (4.20) we used observations collected by Donelan (1982). These data, displayed in Fig. 10a, show the dependence of drag coefficient C_{10} on wind velocity u_{10} for different wave ages. The same values of drag coefficient are presented in Fig. 10b as a function of parameter R.

The Phillips parameter α included in R was estimated by formula (4.7), which can be presented in the form

$$\alpha = 0.57(C_{10}^{1/2}u_{10}/c_p)^{3/2}. \tag{4.20}$$

Values of C_{10} and u_{10} were given by Donelan (1982).

The scatter on nondimensional scale R in Fig. 10b is noticeably less than that in Fig. 10a.

The calculation of input term $\mathcal{E}$ at frequency ω and angle $\theta - \theta_w$ to the wind may be performed knowing the wind velocity u_h at arbitrary height h by the following steps:

(a) assigning the initial value of drag coefficient C_h;
(b) calculation of the friction velocity v_*;
(c) calculation of parameter α [formula (4.7)];
(d) calculation of parameter R [formula (4.18)];
(e) calculation of the drag coefficient C_h [formula (4.19)];
(f) return to item (b) for iterations (one iteration is usually enough to reach a good accuracy);
(g) calculation of the apparent wavelength λ_a [formula (2.6)];
(h) calculation of the total roughness parameter z_0, u_λ, and C_λ using the relations

$$z_{0t} = h \exp(-kC_h^{-1/2}), \tag{4.21}$$

$$u_\lambda = u_h \frac{\ln(\lambda_a/z_0)}{\ln(h/z_0)}, \tag{4.22}$$

$$C_\lambda = C_h(u_h/u_\lambda)^2, \tag{4.23}$$

(i) calculation of the nondimensional frequency ω_a [formula (2.5)];
(j) calculation of the β-parameter as a function of C_λ and $\tilde{\omega}_a$ (see ChB93);
(k) calculation of the spectral density of energy input $\mathcal{E}$ by formula (2.16).

5. Concluding Remarks

The aim of this paper is a formulation of a parameterization scheme for the WBL in coupled atmosphere–wave models. The scheme is based on the nonstationary momentum equations (2.1)–(2.3), the stationary turbulent equation (2.14), and boundary conditions (3.1) [or (3.2)] and (3.24).

The scheme of energy input described above together with a new scheme for wave energy dissipation has been implemented into an experimental third-generation WAVEWATCH model (Tolman 1991) at National Meteorological Center.

Further development of the WBL theory should be performed in three main directions.

1) The direct modeling of the statistical structure of the WBL using 2D and 3D Reynolds equations (Chalikov 1986) should be attempted. We are not sure that the β function is established accurately enough for high frequencies and large drag coefficients, so it is necessary to perform a new series of 2D and 3D simulations. The 3D approach may be extended by implementation of the large eddy-scale simulation technique. The most important problem is the establishment of the precise form of the wind–wave interaction parameter and the WPMF profile in a broad range of frequencies. The conception of the local drag law also needs a further investigation.

2) It is clear now that the wind–wave interaction problem is much more complicated than it originally seemed, because the WPMF cannot be represented, in fact, as a simple decomposition of elementary fluxes produced by monochromatic waves. Although we are forced to use this assumption, in reality all waves influence the wind profile and the energy and momentum exchange.

All previous investigations of WBL used the condition of the water surface as a superposition of linear waves. Thus, the nonlinear nature of surface waves was ignored. A much more consistent approach should be developed by joining the WBL model with the nonlinear wave model (Chalikov and Liberman 1991) describing the individual wave dynamics. In a 2D approach the most appropriate method is based on conformal (surface following) mapping of domain. This transformation is especially effective for potential wave equations. A two-layer approach may offer deeper insight into physics of small-scale wind–wave interaction. Unfortunately, this approach also suffers from grave shortcomings. First, the potential waves cannot be influenced by tangential stress. Second, many important phenomena including wave breaking cannot be reproduced in full in potential approximation. Probably the effect of wave breaking may be parameterized on the basis of instability criterias and considerations of momentum and energy balance.

The main advantage of potential approach is that it allows one to reduce the problem by one dimension. The simulation of nonpotential waves over long period is practically impossible because the evolution of energy due to inaccuracy in approximation of vertical derivatives exceeds the rate of nonlinear wave–wave interaction.

3) The coupled atmosphere–ocean simulation should be extended by joining with WAM-type and WBL models. Only this approach would allow one to reproduce a closed balance of momentum and energy in a wind-wave–mixed layer system.

Acknowledgments. The author thanks Drs. P. E. Long and W. Perrie, who read the manuscript and gave many valued comments, and also Dr. L. Lobocki and R. Teboulle for help in the visualization of results. This paper was written during work at the National Meteorological Center, Development Division, Marine Prediction Branch. The author is indebted Dr. E. Kalnay and Dr. D. B. Rao for their encouragement.

REFERENCES

Blake, R. A., 1991: The dependence of wind stress on wave height and wind speed. *J. Geophys. Res.*, **96,** 531–545.

Chalikov, D., 1976: A mathematical model of wind-induced waves. *Dokl. Akad. Nauk SSSR,* **229,** 1083–1086.

——, 1978: The numerical simulation of wind–wave interaction. *J. Fluid Mech.*, **87,** 561–582.

——, 1986: Numerical simulation of the boundary layer above waves. *Bound.-Layer Meteor.*, **34,** 63–98.

——, 1993: Comments on "Wave-induced stress and the drag of air flow over sea waves" and "Quasilinear theory of wind-wave generation applied to wave forecasting." *J. Phys. Oceanogr.*, **23,** 1597–1600.

——, and Y. M. Liberman, 1991: Integration of the full equations of potential waves. *Izv. Atmos. Oceanic Phys.* (English Transl.), **27**(11); 898–902.

——, and V. Makin, 1991: Models of the wave boundary layer. *Bound.-Layer Meteor.*, **56,** 83–99.

——, and M. Y. Belevich, 1993: One-dimensional theory of the wave boundary layer. *Bound.-Layer Meteor.*, **63,** 65–96.

Charnock, H., 1955: Wind stress on a water surface. *Quart. J. Roy. Meteor. Soc.*, **81,** 639.

Donelan, M. A., 1982: The dependence of the aerodynamic drag coefficient on wave parameters. *Proc. First Int. Conf. on Meteor. and Air–Sea Interaction of the Coastal Zone,* The Hague, the Netherlands, Amer. Meteor. Soc., 381.

Garratt, J. R., 1977: Review of drag coefficient over oceans and continent. *Mon. Wea. Rev.*, **105,** 915–929.

Gent, P. R., 1977: A numerical study of air flow above water waves. Part 2. *J. Fluid Mech.*, **82,** 349–369.

——, and P. A. Taylor, 1976: A numerical model of air flow above water waves. *J. Fluid Mech.*, **77,** 105–128.

Glazman, R. E., and S. H. Pilorz, 1990: Effect of sea maturity on satellite altimeter measurements. *J. Geophys. Res.*, **95**(C3), 2857–2870.

Hasselmann, D. E., M. Dunckel, and J. A. Ewing, 1980: Directional wave spectra observed during JONSWAP 1973. *J. Phys. Oceanogr.*, **10,** 1264–1280.

Hasselmann, K., and Collaborators, 1973: Measurements of wind–wave growth and swell decay during the Joint Sea Wave Project (JONSWAP). *Dtsch. Hydr. Z.*, **A8**(12), 95 pp.

Janssen, P. A. E. M., 1989: Wind-induced stress and the drag of air flow over sea waves. *J. Phys. Oceanogr.*, **19,** 745–754.

Jenkins, A. D., 1992: A quasi-linear eddy-viscosity model for the flux of energy and momentum to wind waves using conservation-law equations in a curvilinear coordinate system. *J. Phys. Oceanogr.*, **22,** 843–858.

Kitaigorodskii, S. A., 1962: Application of the theory of similarity to the analysis of wind-generated motion as a sto-

chastic process. *Bull. Acad. Sci.,* USSR Geophys. Ser. 1, 105–117.

Panchenko, E. G., and D. V. Chalikov, 1984: The energy structure of the atmospheric boundary layer above waves. *Izv. Atmos. Oceanic Phys.* (English transl.), **20,** 732–737.

Smith, S. D., and E. G. Banke, 1975: Variation of the sea surface drag coefficient with wind speed. *Quart. J. Roy. Meteor. Soc.,* **101,** 665.

——, R. J. Anderson, W. A. Oost, C. Kraan, N. Maat, J. DeCosmo, K. B. Katsaros, K. L. Davidson, K. Bumke, L. Hasse, and H. M. Chadwick, 1992: Sea surface wind stress and drag coefficients: The HEXOS results. *Bound.-Layer Meteor.,* **60,** 109–142.

Tolman, H. L., 1991: A third-generation model for wind waves on slowly varying, unsteady, and inhomogeneous depth and currents. *J. Phys. Oceanogr.,* **21,** 782–797.

Wu, J., 1980: Wind-stress coefficient over sea surface near neutral conditions—A revisit. *J. Phys. Oceanogr.,* **10,** 727–740.

——, 1988: Wind-stress coefficient at light winds. 1988: *J. Atmos. Oceanic Technol.,* **5,** 885–888.

Yuen, H. C., and B. M. Lake, 1982: Non-linear dynamics of deep-water gravity waves. *Advances in Applied Mechanics,* Vol. 22, Academic Press, 67–229.